

Distribution of the magnetic flux in elements of the magnetic field in active regions

V.I. Abramenko

Big Bear Solar Observatory, 40386 N. Shore Lane, Big Bear City, CA 92314, USA
Crimean Astrophysical Observatory, 98409, Nauchny, Crimea, Ukraine

and

D.W. Longcope

Department of Physics, Montana State University, Bozeman, MT 59717

ABSTRACT

The unsigned magnetic flux content in flux concentrations in two active regions are calculated by using a set of 248 high resolution SOHO/MDI magnetograms for each active region. Data for flaring active region NOAA 9077 (July 14, 2000) and non-flaring active region NOAA 0061 (Aug 09, 2002) were analyzed. We present an algorithm to automatically select and quantify magnetic flux concentrations above a threshold p . Each active region is analyzed using 4 different values of the threshold, p ($p = 25, 50, 75$ and 100 G). Probability distribution functions (PDFs) and cumulative distribution functions (CDFs) of the magnetic flux were calculated and approximated by the log-normal, exponential and power law functions in the range of flux $\Phi > 10^{19}$ Mx. The Kolmogorov-Smirnov test applied for each of the approximations, showed that the observed distributions are consistent with the log-normal approximation only. Neither exponential, nor power law functions can approximate satisfactory the observed distributions. The parameters of the log-normal distribution do not depend on the threshold value, however they are different for the two active regions. For flaring active region 9077, the expectation value of the magnetic flux content is $\mu = 28.1 \times 10^{18}$ Mx and the standard deviation of the log-normal distribution, $\sigma = 79.0 \times 10^{18}$ Mx. For non-flaring active region NOAA 0061 these values are: $\mu = 23.8 \times 10^{18}$ Mx and $\sigma = 29.6 \times 10^{18}$ Mx. The log-normal character of the observed distribution functions suggests that the process of fragmentation dominates over the process of concentration in the formation of the magnetic structure in an active region.

Subject headings: Sun: magnetic field; magnetic elements; distribution function

1. Introduction

Magnetic fields in the solar atmosphere are thought to be concentrated in thin flux tubes anchored in the photosphere, where their footpoints form concentrated clusters of magnetic flux. Turbulent flows in the photospheric plasma braid and intertwine the flux tubes causing one of the mechanisms for the heating of the corona (Parker 1996, see Priest & Forbes 2000 for references). Information on the dynamics and statistical characteristics of the photospheric magnetic field is necessary when analyzing processes in the corona due to the magnetic coupling between the photosphere and the corona. Some of these studies include: analysis of generation and propagation of waves in the solar atmosphere (Thomas & Stanchfield 2000, Bogdan et al. 2003); modeling of coronal heating (Gudiksen & Nordlund 2002, Fludra & Ireland 2003), exploration of the magnetic coupling between the photosphere and the corona (Handy & Schrijver 2001, Bewsher et al. 2002, Moore et al. 2003). In addition, such information is usually used as input parameters and/or diagnostic criteria in the modeling of the interaction between the turbulent plasma and the magnetic field in the convective zone and in the photosphere (Petrovay & Szakaly 1993, Tao et al. 1995, Schrijver et al. 1997a, Fan et al. 2003, Longcope et al. 2003, Janßen et al. 2003); in the solar dynamo models (Cadavid et al. 1994, Lawrence et al. 1995, Stein & Nordlund 2002), small-scale turbulent dynamo action (Cattaneo et al. 2001) and in modeling of magnetic reconnection in solar flares (Longcope & Noonan 2000, Hood et al. 2002).

Recently, Longcope et al. (2003) proposed a viscoelastic theory of the interaction between turbulent flows and fibril magnetic fields, which is capable of resolving the "dynamo quenching" problem and of explaining how a mean field dynamo operating on fibril fields can produce flux tubes of field strength exceeding turbulent equipartition strength. The model is based on an assumption of the back-reaction of the fibrils (magnetic flux tubes) on the plasma flow. All aspects of the back-reaction depend on the distribution function of magnetic flux in fibrils.

Modern observational technique allows us to calculate the distribution function of flux concentrations of the magnetic field at the photospheric level only. In quiet Sun areas, where the flux concentrations are widely separated, the concentrations can be determined much more easy than in an active region area, where they are tightly packed. As a consequence, studies of the distribution of magnetic flux in quiet sun regions are more popular. Thus, Wang et al. (1995) studied the dynamics and statistics of the network and intranetwork magnetic fields using Big Bear Solar Observatory videomagnetograph data. The authors argued that the distribution function follows a power law. They found a power index of -1.68 for areas whose flux was in the range $(0.2 - 1) \times 10^{18}$ Mx (intranetwork fields) and -1.27 for areas whose flux was in the range $(2 - 10) \times 10^{18}$ Mx (network elements).

Schrijver et al. (1997a) used high resolution data from the Michelson Doppler Imager (MDI) on-board SOHO of a quiet network area. They reported that the flux distribution function follows an exponential law with a slope of approximately $1 \times 10^{-18} \text{ Mx}^{-1}$ in areas where the flux ranges from 1 to $5 \times 10^{18} \text{ Mx}$. The distribution of magnetic flux in flux concentrations in a plage area (outside of large sunspots) of active region NOAA 7962 also was analyzed by Schrijver et al. (1997b). The authors reported that the distribution function in the plage areas is less steep than that for the quiet sun, with the exponential slope slightly varying as a function of the flux. To explain the shape of the observed distribution, the authors modeled the distribution of flux concentrations assuming that three primary processes underlie the creation of the distribution of flux concentrations. Namely, merging, cancellation and fragmentation of flux concentrations. Under this assumption, the exponential slope should vary with the inverse proportion to the square root of the average flux density, and so a satisfactory agreement between the observed and modeled distributions in the range $(20 - 150) \times 10^{18} \text{ Mx}$ was reached.

In the present study, we calculate and analyze the distribution of magnetic flux concentrations in the two well developed active regions in the range of flux $\Phi > 10^{19} \text{ Mx}$. We payed special attention to the analytical approximation of the observed distribution.

2. Observational data

We analyzed SOHO/MDI high-resolution line-of-sight magnetograms (Scherrer et al. 1995) of two active regions. The data for the first one, NOAA 9077, were obtained on July 14, 2000 (Figure 1). At this day, this mature active region produced the famous Bastille day flare of X5.7 X-ray class. About 130 flares occurred during its disk passage on the Sun.

The second active region NOAA 0061 was observed on Aug 9, 2002 (Figure 2). This moderate active region produced several C-class flares during the passage across the solar disk. During the time period analyzed here, this active region produced no flares, as well as several hours before and after.

During the MDI observations, both active region were located near the center of the solar disk. Therefore the measured line-of-sight component of the magnetic field very closely represents a component B_z , normal to the solar surface. For each active region, we used a sequence of 248 magnetograms obtained between 06:26 UT and 11:00 UT in the case of NOAA 9077 and between 11:00 UT and 15:22 UT in the case of NOAA 0061. We studied an area 145×145 arc sec (250×250 pixels, Figure 1) for AR 9077 and an area 380×200 pixels for AR 0061 (Figure 2).

The scale of the MDI magnetograms is 0.58 arcsec which provides a spatial resolution of approximately 1.2 arcsec. We applied a 3-pixel running mean procedure in the horizontal and vertical directions to each magnetogram before identifying concentrations.

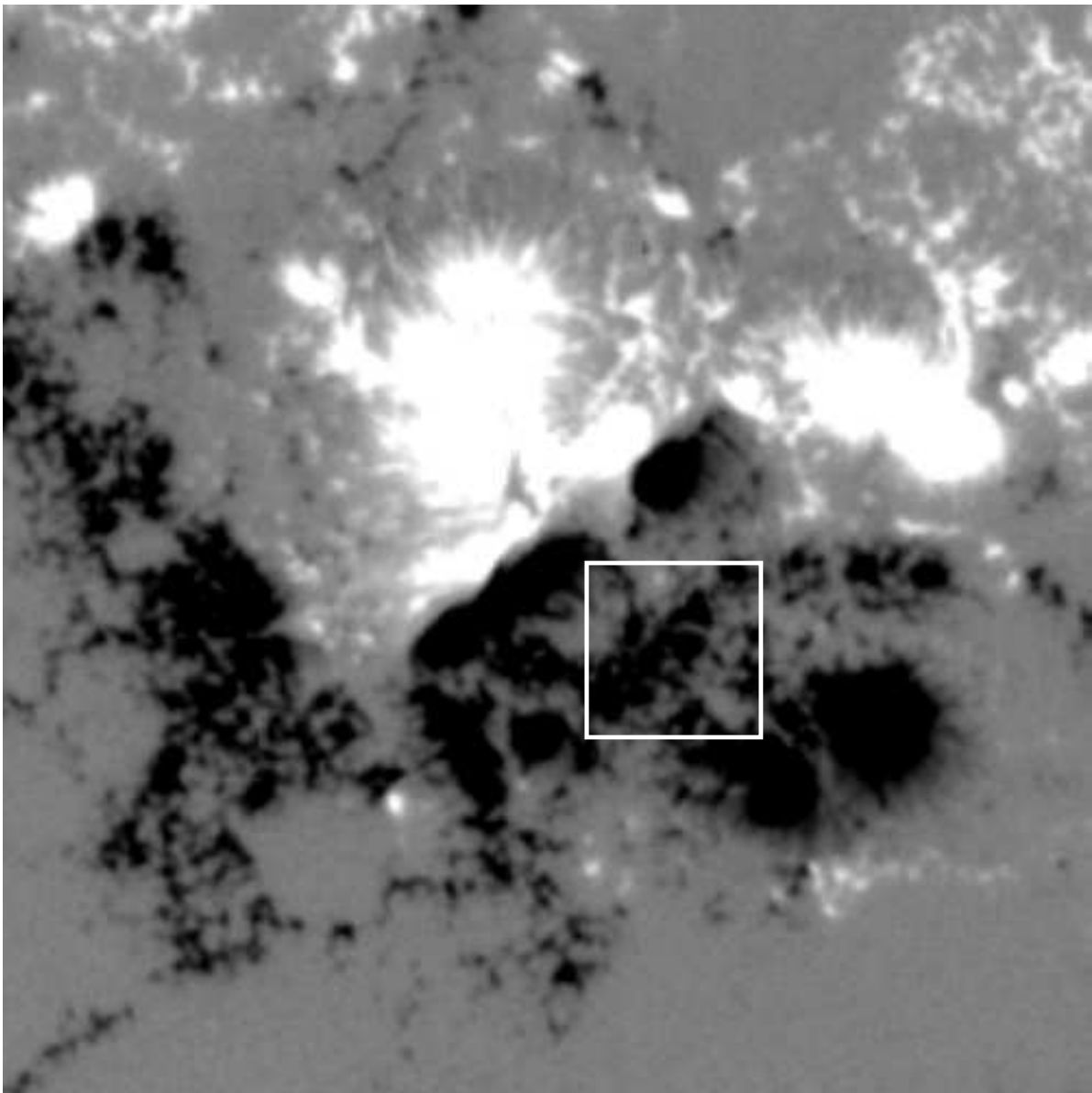


Fig. 1.— A high-resolution SOHO/MDI magnetogram of active region NOAA 9077 obtained on July 14, 2000 at 06:26 UT. The size of the magnetogram is 145×145 arc sec. The intensity of the image is scaled within a range of ± 900 G. The white box encloses an arbitrary area, enlarged in Figure 3, which we used to explain our code. North is to the top and west is to the right.

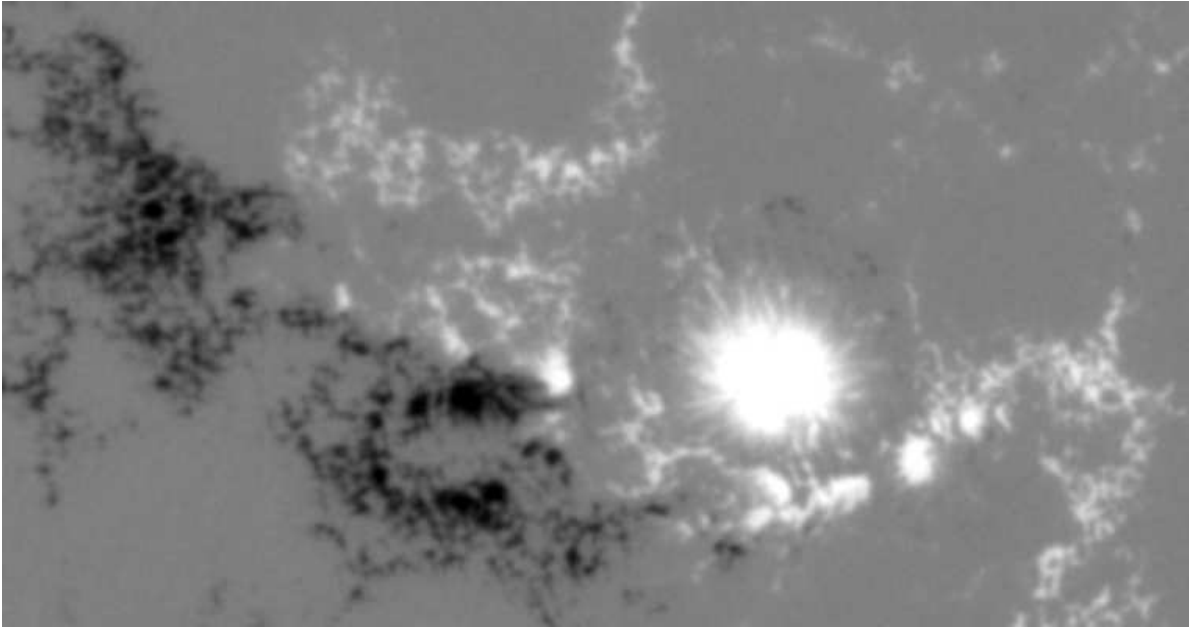


Fig. 2.— A high-resolution SOHO/MDI magnetogram of active region NOAA 0061 obtained on Aug 9, 2002 at 11:00 UT. The size of the magnetogram is 220×116 arc sec. The intensity of the image is scaled within a range of ± 900 G. North is to the top and west is to the right.

3. Specification of a threshold in the magnetograms

To determine the magnetic concentrations on a magnetogram, one of the most important, and most uncertain, question is the choice of a threshold to determine the boundary of the concentrations. We assume that if the absolute value of B_z in a given pixel exceeds the threshold, p , then the pixel belongs to a flux concentration.

We selected four values for the threshold: 25, 50, 75 and 100 G. Our estimate of the noise in a quiet area of a magnetogram showed that the r.m.s. corresponds approximately to 17 G, in a good agreements with the detection limit for the magnetic flux density from the MDI high resolution data reported by Schrijver et al. (1997b). Thus, a threshold of 50 G corresponds approximately to the 3σ level of the noise. We consider this threshold, as well as larger and smaller values in order to assess the affect of its choice.

Our selection of the threshold values agrees with a solution of the same problem in previous studies. Balke et al.(1993) used data obtained with the Vacuum Tower Telescope of the Swedish Solar Observatory on La Palma, to calculate the fractal dimension of the magnetograms. The noise level was estimated to be 180 G, and the authors chose a threshold higher than 200 G. Janßen et al. (2003) specified a threshold of 50 G as the detection limit for determination of magnetic flux densities by using the Vacuum Tower Telescope (Tenerife) data. Meunier (1999) used a set of the threshold values ranging from 40 to 200 G to study the fractal dimensions of the magnetograms from MDI (full disk and high resolution) data. Schrijver et al. (1997b) chose a threshold of 50 G to calculate the distribution of magnetic flux concentrations in the plage area by using the SOHO/MDI high resolution (HR) magnetograms. The threshold value about 45 G was chosen by Schrijver et al. (1997a) to analyze the photospheric quiet network magnetic flux by using the MDI/HR data.

4. The routine to select magnetic flux concentrations in a map

We assumed that a pixel belongs to a magnetic flux concentration when the absolute value of the magnetic field contained therein exceeds the threshold, i.e. $|B_z| > p$. Thus, we did not separate magnetic polarities and study only the absolute values of the magnetic flux content in concentrations (unsigned flux content).

We determined the local peak of a concentration as a pixel where both, $d|B_z|/dx$ and $d|B_z|/dy$, change their sign from plus to minus (here x and y are the coordinates on the magnetogram). Each peak in a magnetogram was labeled. The positions of the local peaks are indicated by white diamonds in Figure 3. The background in the figures is an

enlarged arbitrary area marked by the box in Figure 1. Our next step was to outline the flux concentrations and to calculate their flux content.

In the case when the unsigned flux density of a given pixel exceeds the threshold, our code determines to which peak a given pixel belongs by moving in a direction of the maximum gradient on the map of $|B_z|$. When we encounter a pixel labeled as a peak, we summed the flux and the area of the current pixel to the total flux and total area of a given flux concentration. Note, that this routine is analogous to that proposed by Hagenaar et al. (1997) to calculate the size of elements of the chromospheric network.

The result of the application of the code to the arbitrary fragment of a magnetogram of 40×40 pixels is shown in Figure 3. Although the threshold level was highest in this example (100 G), the flux concentrations are packed very close to each other (side by side) while the dividing lines between the concentrations run along "valleys".

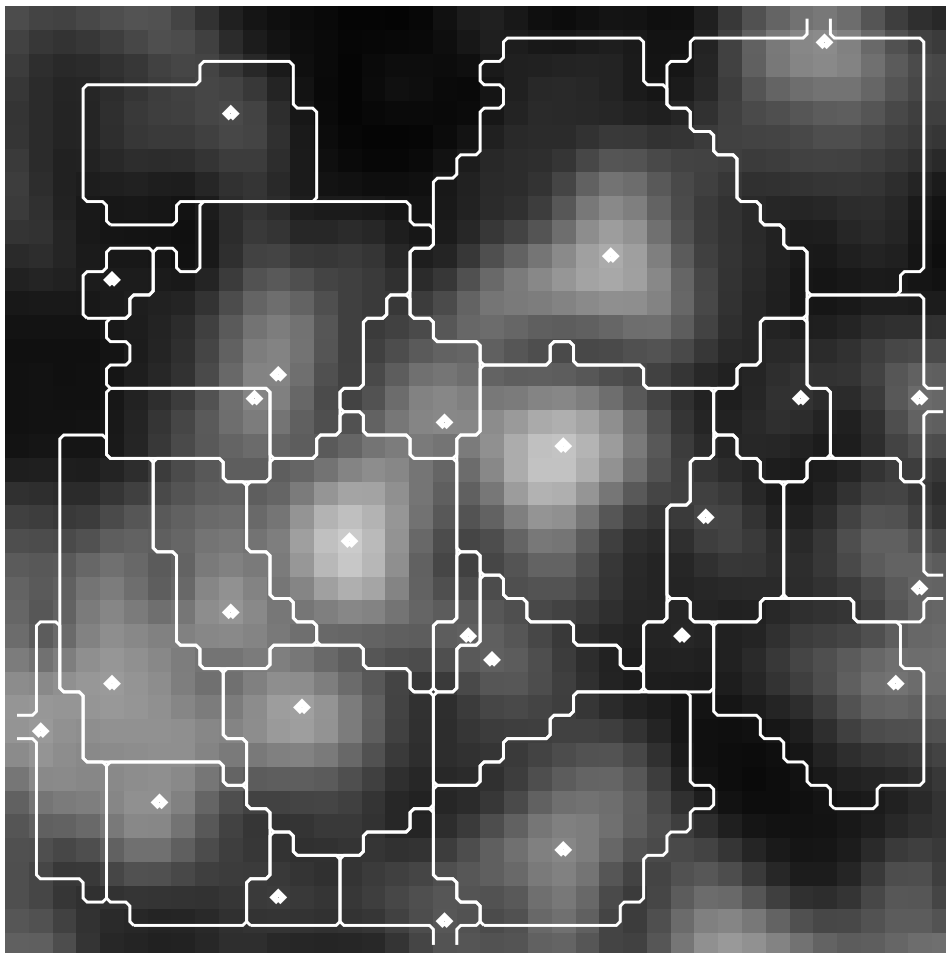


Fig. 3.— A map of the absolute value of the magnetic field, B_z , for the area enclosed by the box in Figure 1. The image is scaled in the range of values 0 – 1200 G . The white diamonds mark the position of the peaks of flux concentrations. The white lines outline the boundaries between the flux concentrations.

5. Calculations of distribution functions of magnetic flux concentrations

We performed a statistical analysis of the magnetic flux concentrations in two active regions for each level of the threshold $p = 25, 50, 75, 100$ G. In each magnetogram we determined approximately 600-800 concentrations, depending on the threshold value. To calculate a histogram of the magnetic flux, Φ , we have to specify a flux range where we want to obtain the histogram and the number of bins. For the great majority of the concentrations (for both active regions) the absolute value of the magnetic flux did not exceed 8×10^{20} Mx. We accepted this value as the upper limit of the flux range for the histogram. We then chose the number of bins equal to $n = 3000, 2500, 2000, 1600$ for the threshold values $p = 25, 50, 75, 100$ G, respectively, so that the total number of concentrations in 248 magnetograms, N , divided by the number of bins, n , was approximately the same for different thresholds. For each magnetogram of a given active region, we calculated the histogram of the magnetic flux content in the flux concentrations. After normalizing each histogram for the total number of concentrations in the magnetogram, we averaged these normalized histograms over the total number of magnetograms, thus obtaining the averaged probability distribution function, $PDF(\Phi)$. For the active region 9077, the PDF from 248 magnetograms is shown by thick gray line in the top panels in Figures 5-7.

To apply an analytical approximation to the observed distribution function, one has to determine the lower value of the magnetic flux, Φ_{cut} , below which the calculated values of flux may be significantly affected by influence of noise, threshold, resolution, etc. Figure 4 shows the magnetic flux content, Φ , versus the mean magnetic flux density, $\langle |B_z| \rangle$, in the flux concentrations of an arbitrary magnetogram of active region 9077 calculated for the threshold of 50 G. A sharp lower edge in the distribution of data points suggests a lower cut-off in $\langle |B_z| \rangle$ curving upward from approximately 50 G. At fluxes $\Phi < 10^{19}$ Mx, data points are tightly clustered against this artificial limit, suggesting that the choice of threshold has eliminated or compromised some data. The situation is the same for the second active region (NOAA 0061) and for other thresholds. Thus, we chose $\Phi_{cut} = 10^{19}$ Mx as flux cut-off above which we believe our sample is reasonably complete.

For an arbitrary magnetogram of each active region, we calculated the cumulative distribution function (CDF) for flux values $\Phi > \Phi_{cut}$. The function $CDF(\Phi)$ giving the fraction of all concentrations with flux greater than Φ , does not require a bin size be defined. The result for active region 9077 is shown in the bottom panels of Figures 5-7. The dark curve on this plot is the CDF whose corresponding PDF is the fit to the average of all 248 PDFs.

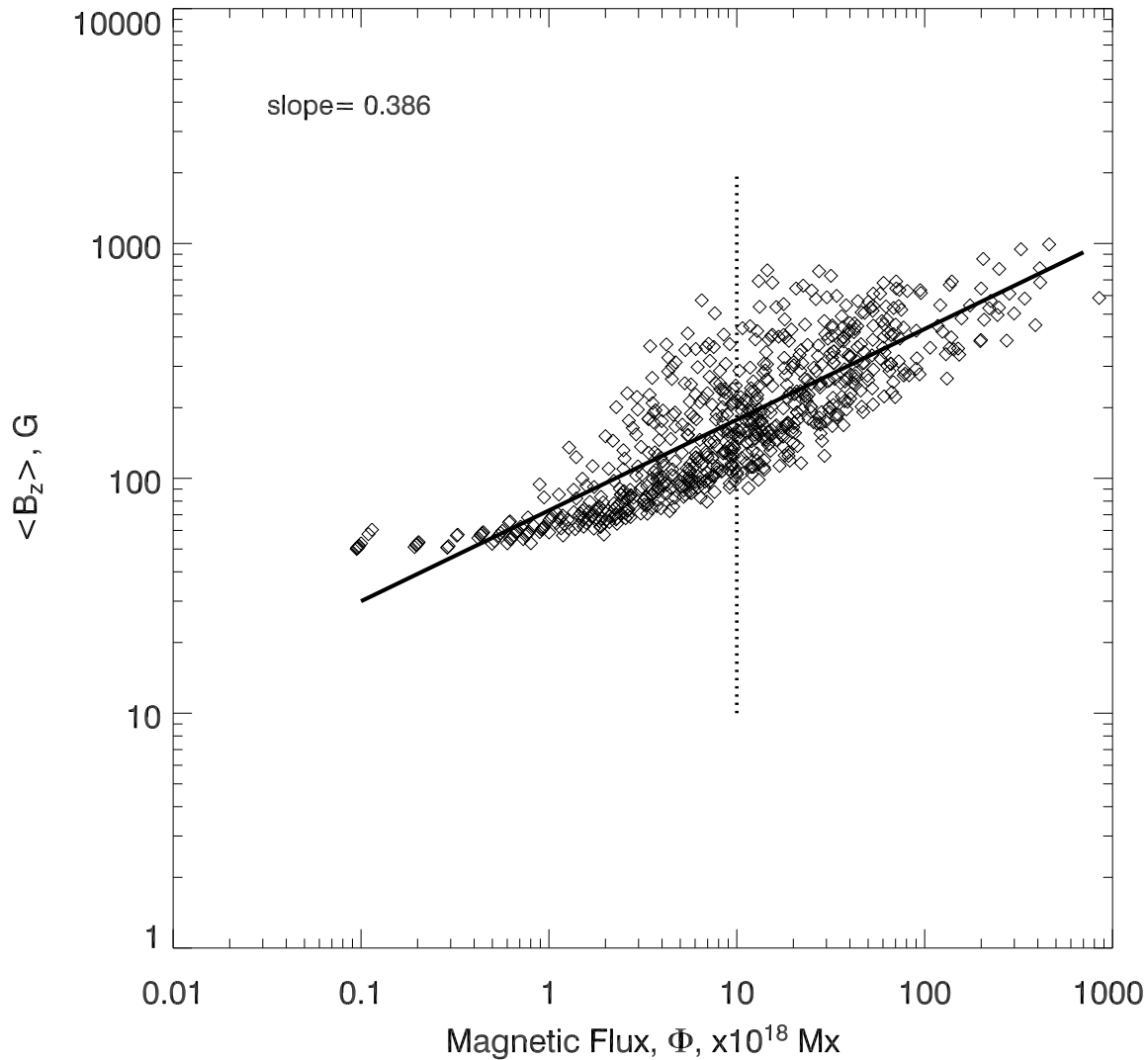


Fig. 4.— Averaged (over the area) magnetic field density, $\langle |B_z| \rangle$, versus the magnetic flux content, Φ , for the magnetic flux concentrations from the magnetogram of AR NOAA 9077 obtained at 08:12 UT on July 14, 2000. The threshold is 50 G. The vertical dotted segment corresponds to $\Phi = \Phi_{cut} = 10^{19}$ Mx, i.e. the accepted value of the flux cutoff, below which the diagram is artificially distorted. The linear best fit (the slope of 0.386 and the correlation coefficient of 0.606) over the range $\Phi > \Phi_{cut}$ is marked by the solid line.

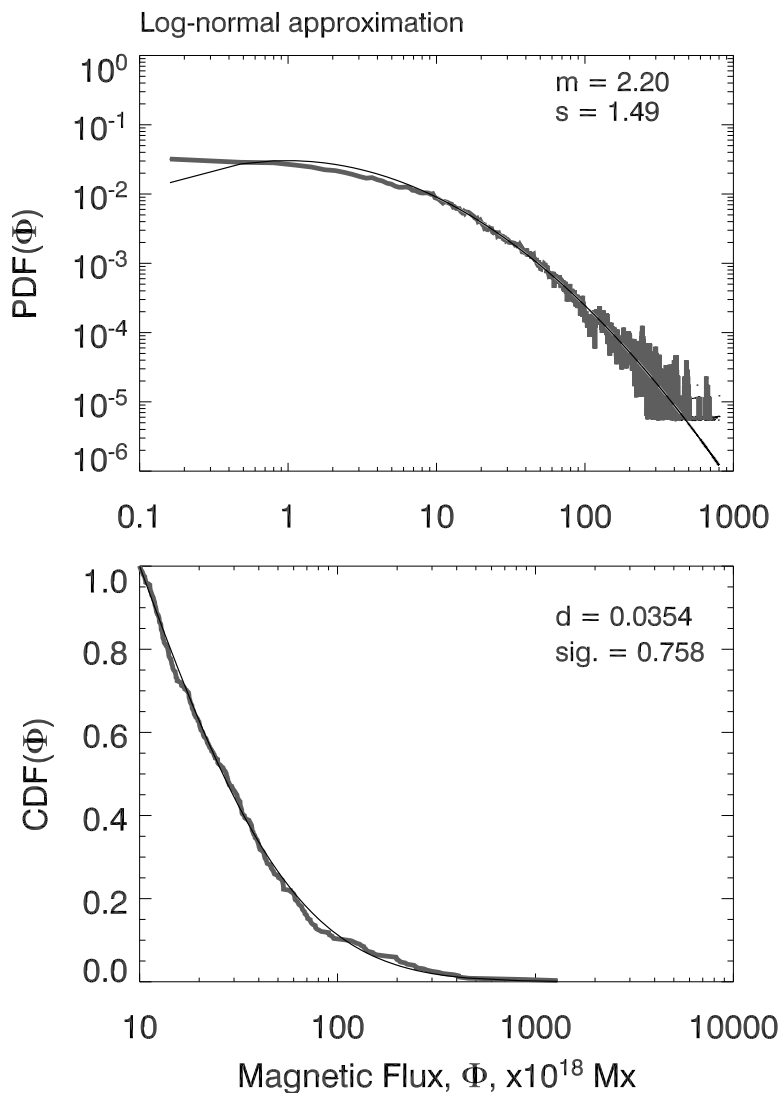


Fig. 5.— *Top* - Observed probability distribution function (PDF) of the magnetic flux in flux concentrations of active region NOAA 9077 (the thick gray line) determined for the threshold of 50 G. The PDF is calculated as the average from individual PDFs for each of 248 magnetograms. The thin black curve marks the log-normal function with parameters m and s calculated as a best fit over the flux range $\Phi > 10^{19}$ Mx. *Bottom* - Observed cumulative distribution function (CDF, the thick gray line) calculated in the flux range $\Phi > 10^{19}$ Mx from the magnetogram of active region NOAA 9077 obtained at 08:12 UT on July 14, 2000. The thin black curve marks the log-normal function, $LN(m, s)$, with parameters $m = 2.20$ and $s = 1.49$, as they were obtained from the PDF. The parameters of Kolmogorov-Smirnov test (d and significance, sig) between $LN(m, s)$ and observed CDF, are noted.

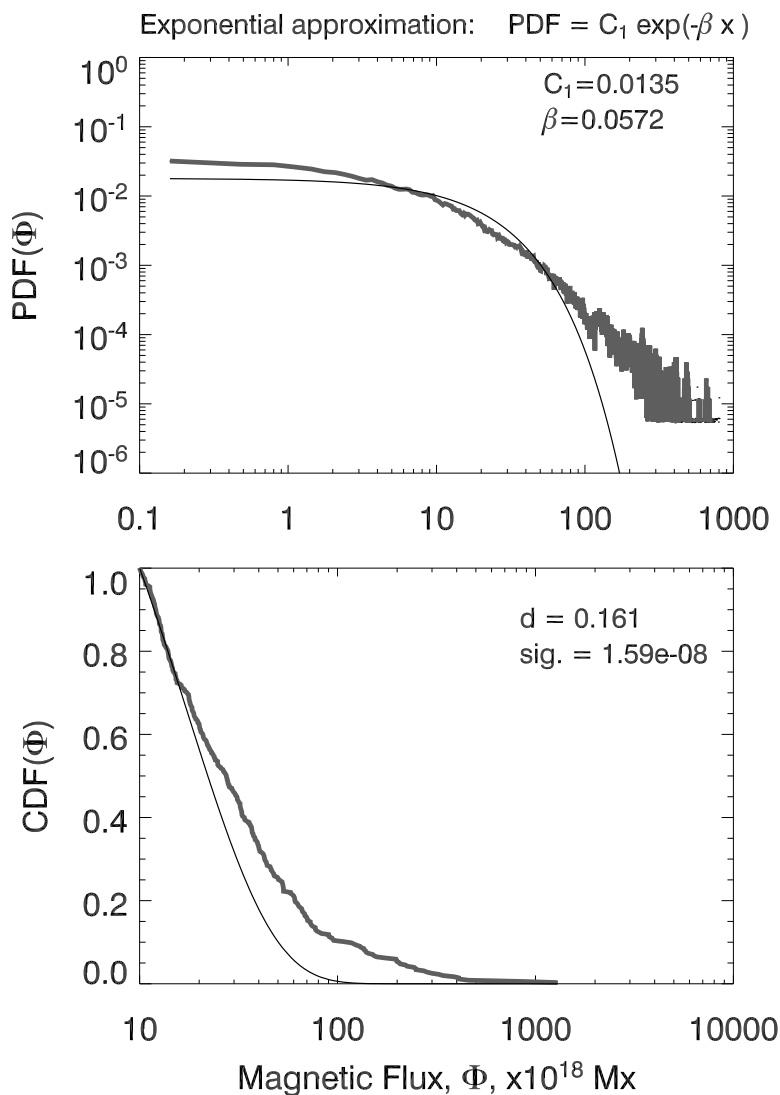


Fig. 6.— Exponential approximation to the observed distribution functions shown in Fig. 5. The parameters C_1 and β , in accordance with eq.(4), are shown. The thin black curves in both panels show the exponential function with $C_1 = 0.0135$ and $\beta = 0.0572$, calculated as a best fit to the PDF over the flux range $\Phi > 10^{19}$ Mx. Other notations are the same as in Figure 5. Note the very low level of significance of Kolmogorov-Smirnov test between the exponential fit and the observed CDF.

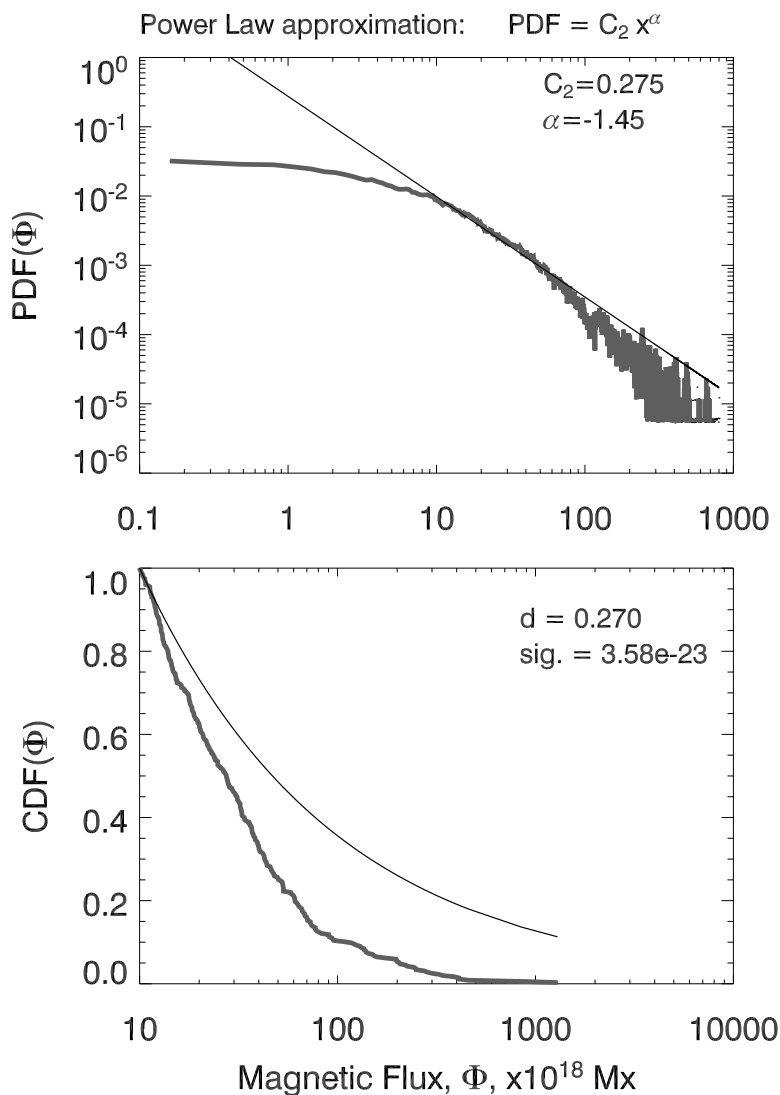


Fig. 7.— Power law approximation to the observed distribution functions shown in Fig. 5. The parameters C_2 and α , in accordance with eq.(5), are shown. The thin black curves in both panels show the power law function with $C_2 = 0.275$ and $\beta = -1.45$, calculated as a best fit to the PDF over the flux range $\Phi > 10^{19}$ Mx. Other notations are the same as in Figure 5. The level of significance, sig. , of Kolmogorov-Smirnov test between the power law fit and the observed CDF, is extremely low.

6. Approximation for the observed distributions

To quantitatively analyze the obtained distributions, we attempted to fit the PDF to three different distributions: log-normal, exponential and power law.

In the first possibility, a log-normal distribution (Aitchison & Brown 1957, Romeo et al, 2003), the logarithm of the magnetic flux is normally distributed. This makes the PDF of Φ

$$PDF(\Phi) = \frac{1}{\Phi s(2\pi)^{1/2}} \exp \left[-\frac{1}{2} \left(\frac{\ln(\Phi) - m}{s} \right)^2 \right], \quad (1)$$

for $\Phi > 0$. The function's two parameters m and s are the mean and standard deviation of $\ln(\Phi)$. The expectation value, μ , and the variance, σ^2 , of log-normally distributed flux are defined in terms of these parameters

$$\mu = \exp \left(\frac{2m + s^2}{2} \right), \quad (2)$$

$$\sigma^2 = \exp(2m + 2s^2) - \exp(2m + s^2). \quad (3)$$

The mean flux, μ , exceeds the *median* flux, e^m , by a factor $e^{s^2/2}$, which can be far greater than unity for large values of s . In the opposite limit, $s \ll 1$, the log-normal distribution approaches a Gaussian (normal) distribution and the mean approaches the median.

The average PDF was fit to expression (1) by performing a standard, unweighted least-squares Gaussian fit to the function $\Phi \cdot PDF(\Phi)$ versus $\ln(\Phi)$. The mean and standard deviation of this fit yield the parameters m and s . Values for each active region for different threshold values are listed in Table 1. A typical example of the log-normal approximation in the range $\Phi > \Phi_{cut}$ is shown in Figure 5.

The second possibility, an exponential distribution, corresponds to the PDF

$$PDF(\Phi) = C_1 \exp(-\beta\Phi), \quad (4)$$

where $C_1 = \beta e^{\beta\Phi_{cut}}$ when using the range $\Phi > \Phi_{cut}$. We calculate β as the negative slope when $\ln(PDF)$ is fit, by unweighted least-squares, to a linear function of Φ . Our data for AR NOAA 9077 gave the value $\beta \approx 0.036 \times 10^{-18} \text{ Mx}^{-1}$ which $\ln(\Phi)$ was fit over the range $(20 - 110) \times 10^{18}$. This agrees well with the value found by Schrijver et al. (1997b) for plage area inside an active region over the same flux range (see Figure 2 in Schrijver et al. 1997b). The results of the exponential approximation are shown in Table 2 and in Figure 6.

The final possibility, a power law distribution, is given by the PDF

$$PDF(\Phi) = C_2 \Phi^{-\alpha}. \quad (5)$$

In an unweighted least-squares fit of $\ln(\text{PDF})$ to a linear function of $\ln(\Phi)$ the slope gives $-\alpha$. Values found from fits to each magnetogram under each of the thresholds is collected in Table 3. An example of the power law fit for the PDF of AR 9077 is shown in Figure 7.

The quality of each fit is quantified using the Kolmogorov-Smirnov (K-S) test. The observed CDF (shown by the thick gray line on the bottom panels of Figs. 5 – 7) is computed from a single arbitrary magnetogram from the active region. The model CDF (thin black line) uses parameters found by fitting the average PDF of the same active region. The K-S statistic d , the maximum absolute deviation between the model and the observed CDF, quantifies the likelihood that the data was drawn from the model distribution (Press et al. 1986). The “significance” is the probability of obtaining a greater value of d if data were randomly drawn from the model distribution. When the significance is smaller than 0.01, for example, we may rule out the proposed model distribution with 99% confidence. The K-S statistic and significance are listed in columns 4 and 5 of Tables 1, 2 and 3 for the three distributions.

The K-S test eliminates, with very high confidence, all distributions except the log-normal. The log-normal distribution is consistent with CDFs from both active regions at every threshold value. It is qualitatively evident from the bottom panels of Figs. 6 and 7 that exponential and power law fits yield poor approximations to the CDFs of a single magnetogram. On the other hand, the log-normal function (Fig. 5) appears to fit the CDF extremely well. We emphasize that the same flux range, $\Phi > 10^{19}$ Mx, was used for each type of distribution in fitting and computing the K-S statistic.

The results above suggest that the magnetic flux in photospheric concentrations is log-normally distributed, at least in the two active regions analyzed. It is noteworthy that the values of the parameters m and s do not depend significantly on the choice of threshold p . Nor do they depend on the choice of flux cut-off: when we lowered the cutoff value, Φ_{cut} , from 10^{19} Mx to 10^{18} Mx, the values of m and s changed no more than by 5 – 6%, while the parameters of the exponential and power law fits changed drastically.

Constructing from Table 1 the threshold-averaged parameters m and s gives direct insight into the structural differences of the two active regions. Average values for active region 9077 are $\bar{m} = 2.244$ and $\bar{s} = 1.478$, which gives us (by eqs. 2 and 3) the expectation and standard deviation of the magnetic flux $\mu = 28.1 \times 10^{18}$ Mx and $\sigma = 79.0 \times 10^{18}$ Mx. For this case, $\bar{s} = 1.478$, the distribution contains large enough tail so that the mean value exceeds the median, $e^{\bar{m}} = 9.4 \times 10^{18}$ Mx by a factor of three. Active region, NOAA 0061, has averaged values $\bar{m} = 2.705$ and $\bar{s} = 0.966$, corresponding to $\mu = 23.8 \times 10^{18}$ Mx and $\sigma = 29.6 \times 10^{18}$ Mx. This is less dominated by its tail and the mean value is only 60% larger than the median.

7. Conclusions and discussion

We have presented the results of fitting the probability distribution function, $\text{PDF}(\Phi)$, of magnetic flux concentrations of two active regions (NOAA 9077 and AR NOAA 0061). We used a set of 248 high resolution SOHO/MDI magnetograms for each active region. The analysis was performed with 4 different threshold values of magnetic flux density (25, 50, 75, 100 G). We fit the averaged PDF, over the range $\Phi > 10^{19}$ Mx, to three different functional forms in turn: log-normal, exponential and power law.

The Kolmogorov-Smirnov test supports the conclusion that only the log-normal distribution is consistent with any of the observed data. Log-normal distributions are consistent with each data set, however, the two active regions are fit by distributions with different parameters.

What can one learn from the distribution of an observed random variable? Some phenomena present a well defined average behavior with fluctuations around the average values. Consider the common case of random variable arising from *sum* of a large number of independent random variables, each of whose fluctuations are small. This variable will exhibit relatively small fluctuations about its mean, and its distribution function will be a narrow Gaussian.

This scenario may be contrasted to a case where the component variables have significant fluctuations. In this case the sum will exhibit large fluctuations. The variable can be said to possess intermittent character, with concentration into small-scale features of high intensity surrounded by extended areas of much lower fluctuations. In this case, the fluctuations are described by a broad distribution function with a slowly diminishing tail, e.g. the log-normal or/and the power law distributions. Intermittent structures arise invariably in the evolution of dynamic systems where dissipative processes may not be neglected.

A natural process for generating a log-normally distributed variable is as a *product*, rather than a sum, of a large number of independent random variables: $u = \prod_i f_i$. In this case $\ln(u) = \sum_i \ln(f_i)$ is the sum of random variables so it will tend to be normally distributed. This is the case when the measured variable arises through *the fragmentation*, or a multiplicative random cascade (see, e.g., Frisch 1995), when some quantity is to be subjected to a large number of random, independent subdivisions.

In the solar photosphere and convective zone, two essential processes determine the interaction between turbulent plasma flows and magnetic flux tubes. On the one hand, a magnetic flux element tends to be advected by the turbulent diffusion. On the other hand, turbulent motions tend to sweep the field lines together at convergence points of

the flow. Fragmentation and concentration are in dynamic equilibrium in homogeneous stationary turbulence. Petrovay & Moreno-Insertis (1997) showed that in inhomogeneous and/or non-stationary situations, turbulent diffusion dominates the concentration causing a turbulent erosion of magnetic flux tubes. The idea of the gradual disintegration of sunspots due to erosion of penumbral boundaries was advanced by Simon & Leighton (1964). Later, Bogdan et al. (1988), on the basis of the observed log-normal distributions of umbral areas, argued that fragmentation of the magnetic elements may be an essential process in the formation of observed magnetic structures. White-light movies of the solar photosphere allow one to observe the erosion of a sunspot (Yurchyshyn & Wang 2001; www.bbso.njit.edu/~vayur/flow/L_981105.mpg). The log-normal distribution of the flux content in magnetic flux elements of an active region suggests that the process of fragmentation dominates the process of flux concentration.

Assuming that the log-normality of concentration flux results from repeated, random fragmentation we may attribute meaning to the distribution parameter. The variance of $\ln(\Phi)$, s^2 , is proportional to the number of independent fragmentations produced a given concentration from a single initial concentration (Monin & Yaglom 1975, Ch.25). If the basic fragmentation process is similar in all active regions then the value of s^2 is proportional to the time over which fragmentation has occurred. Since the value of s^2 for AR 9077 is larger than that of AR 0061, by a factor of 2.3, 9077 may be older than 0061 by approximately that factor. Alternatively, AR 9077 may have undergone more vigorous fragmentation over a comparable lifetime. This explanation may also explain the very different level of their flaring activity (see Section 2). Note, that a very intense fragmentation of sunspots during several days before the Bastille day flare in AR 9077 were reported by Liu & Zhang (2001).

A log-normal distribution with a significant value of s^2 will have a significant tail. This means that the random variable will take on very large values far more often than would a normally distributed variable. These occasional values are large enough that they contribute significantly to the mean value μ , making it far greater than the median. An inverse interpretation of this same fact is that the random variable takes on small values (below the mean) far more often than large ones.

The tendency for values to be well below the mean has an interesting implication for the theory of a viscoelastic back-reaction by fibril fields (Longcope et al. 2003). The stronger coupling of smaller flux tubes to the turbulence gives them stronger fields and therefore smaller volumes. Accounting for this Longcope et al. find the volume-weighted distribution function to be $F(\Phi) \sim \Phi^{5/4} f(\Phi)$ for standard PDFs $f(\Phi)$, such as that given in expression (3). The ensemble of tubes presents an effective viscosity to any slow, large-scale flow. The coefficient of shear-viscosity scales as a product of volume-weighted averages of

inverse powers of Φ , in which the most negative power is $\Phi^{-7/8}$. A log-normal distribution has a greater preponderance of small fluxes than an exponential distribution of the same mean. This means that an ensemble of log-normally-distributed flux tubes will provide viscous back-reaction larger than predictions based on exponential distributions.

We thank Vasyl Yurchyshyn, Haimin Wang and Thomas Spirock for critical comments and helpful discussion of these results. SOHO is a project of international cooperation between ESA and NASA. This work was supported by NSF-ATM 0076602, 0205157, 0233931 and NASA NAG5-12782 grants.

REFERENCES

- Aitchison, J. & Brown, J.A.C., 1957, "The Lognormal Distribution", Cambridge University Press, New York, 176pp.
- Balke, A.C., Schrijver, C.J., Zwaan, C. & Tarbell, T.D., 1993, Sol. Phys. 143, 215
- Bewsher, D., Parnell, C.E., Brown, D.S. & Hood, A.W., 2002, in: SOLMAG 2002. ESA SP-505, 239
- Bogdan, T.J., Gilman, P.A., Lerche, I. & Howard, R., 1988, ApJ. 327, 451
- Bogdan, T. J., Hansteen, M. C. V., McMurry, A., Rosenthal, C. S., Johnson, M., Petty-Powell, S., Zita, E. J., Stein, R. F., McIntosh, S. W. & Nordlund, A., 2003, ApJ, 599, 626
- Cadavid, A.C., Lawrence, J.K., Ruzmaikin, A.A. & Kayleng-Knight, A., 1994, ApJ, 429, 391
- Cattaneo, F., Lenz, D. & Weiss, N., 2001, ApJ, 563, L91
- Fan, Y., Abbett, W.P. & Fisher, G.H., 2003, ApJ, 582, 1206
- Fludra, A. & Ireland, J., 2003, A&A, 398, 297
- Frisch, U. 1995, "Turbulence, The Legacy of A.N. Kolmogorov", Cambridge University Press, 296pp.
- Gudiksen, B.V. & Nordlund, A., 2002, ApJ, 572, L113
- Hagenaar, H.J., Schrijver, C.J. & Title, A.M., 1997, ApJ, 481, 988
- Handy, B.N. & Schrijver, C.J., 2001, ApJ, 547, 1100

- Hood, A. W., Galsgaard, K. & Parnell, C., 2002, in: SOLMAG 2002. ESA SP-505, 285
- Janßen, K., Volger, A. & Kneer, F., 2003, A&A, 409, 1127
- Lawrence, J.K., Cadavid, A.C. & Ruzmaikin, A.A., 1995, Phys. Rev. E, 51,316
- Liu, Y. & Zhang, H. 2001, A&A, 372, 1019
- Londcope, D.W. & Noonan, E.J., 2000, ApJ, 542, 1088
- Longcope,D.W., McLeish, T.C.B. & Fisher, G.H., 2003, ApJ, 599, 661
- Meunier, N. 1999, ApJ, 515, 801
- Monin, A.S. & Yaglom, A.M. 1975, "Statistical Fluid Mechanics: Mechanics of Turbulence",
vol. 2, ed. J.Lumley, MIT Press, Cambridge, MA, 874pp
- Moore, R. L., Falconer, D. A., Porter, J. G. & Hathaway, D. H., 2003, BAAS, 35(3), 826
- Parker, E.N. 1996, Sol. Phys, 169, 327
- Petrovay, K. & Szakaly, G., 1993, A&A, 274, 543.
- Petrovay, K. & Moreno-Insertis, F., ApJ, 485, 398
- Press, W.H., Teukolsky, S.A., Vetterling, S.A., Flannery, B.P. 1986, "Numerical Recipes",
Cambridge Univ. Press, 848p.
- Priest, E. & Forbes, T., 2000, "Magnetic Reconnection", Cambridge University Press, UK,
600pp
- Romeo, M., Da Costa, V. & Bardou, F., 2003, Eur. Phys. J. B, 32, 513
- Schrijver, C.J., Title, A.M., van Ballegooijen, A.A. Hagenaar, H.J. & Shine, R.A., 1997a,
ApJ, 487, 423
- Schrijver, C.J., Title, A.M., Hagenaar, H.J. & Shine, R.A., 1997b, Sol. Phys., 175, 329
- Scherrer, P.H., Bogart, R.S., Bush, R.I., Hoeksema, J.T., Kosovichev, A.G., Schou, J.,
Rosenberg, W., Springer, L., Tarbell, T.D., Title, A., Wolfson, C.J., Zayer, I. and
the MDI engineering team, 1995, Sol. Phys., 162, 129.
- Simon, G.W. & Leighton, R.B., 1994, ApJ, 140, 1120
- Stein, R.F. & Nordlund, A. 2002, in: SOLMAG 2002. ESA SP-505, 83

Tao, L., Du, Y., Rosner, R. & Cattaneo, F., 1995, ApJ, 443, 434

Thomas, J.H. & Stanchfield II, D.C.H., 2000, ApJ, 537, 1086

Wang, J.X., Wang, H., Tang, F., Lee, J.W. & Zirin, H., 1995, Sol. Phys., 160, 277

Yurchyshyn, V.B. & Wang, H., 2001, Sol. Phys. 203, 233

Table 1: Parameters of the log-normal fit to the observed distributions

Threshold, G	m	s	d	sig
Active Region		NOAA 9077		
25	2.113	1.510	0.0389	0.623
50	2.199	1.491	0.0354	0.758
75	2.285	1.472	0.0384	0.681
100	2.378	1.441	0.0344	0.826
Active Region		NOAA 0061		
25	2.690	0.969	0.0445	0.455
50	2.715	0.961	0.0342	0.794
75	2.711	0.965	0.0306	0.906
100	2.703	0.970	0.0427	0.600

Table 2: Parameters of the exponential fit to the observed distributions

Threshold, G	C_1	β	d	sig
Active Region		NOAA 9077		
25	0.0102	0.0593	0.163	4.71e-09
50	0.0135	0.0572	0.161	1.60e-08
75	0.0169	0.0549	0.153	1.50e-07
100	0.0204	0.0523	0.153	3.60e-07
Active Region		NOAA 0061		
25	0.0116	0.0611	0.1130	1.56e-04
50	0.0156	0.0596	0.0953	2.87e-03
75	0.0206	0.0592	0.0966	3.35e-03
100	0.0268	0.0589	0.1057	1.51e-03

Table 3: Parameters of the power law fit to the observed distributions

Threshold, G	C_2	α	d	sig
Active Region		NOAA 9077		
25	0.210	-1.465	0.260	1.65e-22
50	0.275	-1.448	0.270	3.58e-23
75	0.344	-1.432	0.283	1.25e-24
100	0.403	-1.403	0.303	5.63e-27
Active Region		NOAA 0061		
25	0.262	-1.515	0.275	1.03e-24
50	0.348	-1.500	0.288	2.58e-26
75	0.462	-1.499	0.290	1.63e-25
100	0.592	-1.491	0.295	9.07e-25